Infrared spectra of 3-hydroxy -(1H)-pyridinium cation and 3-hydroxy-(1H)-pyridinyl radical isolated in solid *para*-hydrogen

Masashi Tsuge,[1,2,a)] Chia-Peng Lai,[1] and Yuan-Pern Lee[1,3,4,a)]

[1]Department of Applied Chemistry and Institute of Molecular Science, National Chiao Tung University, Hsinchu 30010, Taiwan
[2]Institute of Low Temperature Science, Hokkaido University, Sapporo 060-0819, Japan
[3]Center for Emergent Functional Matter Science, National Chiao Tung University, Hsinchu 30010, Taiwan
[4]Institute of Atomic and Molecular Sciences, Academia Sinica, Taipei 10617, Taiwan

Received: xx, x, 2018; In final form: xx, x, 2018

[a)]Authors to whom correspondence should be addressed. Electronic addresses:

tsuge@lowtem.hokudai.ac.jp and yplee@nctu.edu.tw. Telephone: +886-3-5131459.

KEY WORDS: Infrared spectroscopy, 3-hydroxypyridine, $C_5H_4(OH)NH$, *para*-hydrogen, matrix isolation

ABSTRACT

As pyridine and its derivatives are regarded as building blocks of nitrogen-containing polycyclic aromatic hydrocarbons, spectral identifications of their protonated and hydrogenated species are important. The infrared (IR) absorption spectra of the 3□hydroxy-(1H)-pyridinium cation, 3-$C_5H_4(OH)NH^+$, and the 3-hydroxy-(1H)-pyridinyl radical, 3-$C_5H_4(OH)NH$, produced on electron bombardment during deposition of a mixture of 3□hydroxypyridine, 3-$C_5H_4(OH)N$, and *para*-H_2 to form a matrix at 3.2 K, were recorded. Intense IR absorption lines of *trans*-3-$C_5H_4(OH)NH^+$ at 3594.4, 3380.0, 1610.6, 1562.2, 1319.4, 1193.8, 1167.5, and 780.4 cm^{-1} and eleven weaker ones decreased in intensity after the matrix was maintained in darkness for 20 h, whereas lines of *trans*-3-$C_5H_4(OH)NH$ at 3646.2, 3493.4, 3488.7, 1546.7, 1349.6, 1244.1, 1209.1, 1177.3, 979.8, and 685.2 cm^{-1} and nine weaker ones increased. The intensities of lines of *trans*-3-$C_5H_4(OH)NH$ decreased upon irradiation at 520 nm and diminished nearly completely upon irradiation at 450 nm, whereas those of *trans*-3-$C_5H_4(OH)NH^+$ remained unchanged upon irradiation at 370, 450, and 520 nm. Observed vibrational wavenumbers and relative intensities of these species agree satisfactorily with the scaled harmonic vibrational wavenumbers and IR intensities predicted with the B3LYP/aug-cc-pVTZ method. The observed 3-$C_5H_4(OH)NH^+$ cation and 3-$C_5H_4(OH)NH$ radical are predicted to be the most stable species among all possible isomers by quantum-chemical calculations.

I. INTRODUCTION

Pyridine, C_5H_5N, and its derivatives are important solvents and reagents in organic synthesis and also as precursors of agrochemical and pharmaceutical compounds.[1] Their reactions with acids in the gaseous phase lead to formation of the pyridinium cations.[2] Protonated nitrogen-containing polycyclic aromatic hydrocarbons and their derivatives were proposed to play important roles in interstellar media.[3] Because pyridine and its derivatives serve as building blocks of such nitrogen-containing polycyclic aromatic hydrocarbons, the spectral identifications of their protonated and hydrogenated species are important.

Among common derivatives of pyridine, hydroxypyridines $C_5H_4(OH)N$ are important in organic chemistry and biochemistry because of their critical roles in keto-enol tautomerism;[4, 5] the hydrogen on the oxygen atom of hydroxypyridine can transfer to the nitrogen atom and form pyridone. In biochemical systems, reactions of OH radical with pyridine are important paths for the formation of hydroxypyridines or pyridones.[6] Such keto-enol tautomerism is important for 2-hydroxypyridine and 4-hydroxypyridine because their energies are similar to those of corresponding pyridones.[7, 8, 9, 10] In contrast, 3-hydroxypyridine is more stable than 3-pyridone by 97 kJ mol^{-1} according to quantum-chemical calculations;[11] 3-hydroxypyridine is hence expected to be dominant. Previous investigations established unambiguously that 3-hydroxypyridine exists as a single tautomer in the gaseous phase, as characterized by quantum-chemical calculations,[12, 13, 14, 15, 16, 17] microwave,[18] infrared (IR),[13,19, 20] Raman,[20], photoelectron,[21] and mass spectra.[22, 23, 24] Upon protonation, the 3-hydroxypyridinium cations play important roles in stabilizing some one-dimensional coordination polymers because of the hydrogen-bonded π-π stacking.[25] The 3-hydroxypyridinium cations and uncoordinated water

molecules occupy the inter-chain regions and an N−H••••O bond and numerous O−H••••O hydrogen bonds consolidate the polymer structure.

As a first step to investigate the protonation of the simplest hydroxyl N-containing aromatic hydrocarbons, we chose 3-hydroxypyridine because preparation of protonated and mono-hydrogenated species from this compound is free of complication caused by the existence of two or more tautomers of the parent heterocycle.

Seven sites are possible for the protonation of 3-hydroxypyridine, in contrast to only four possible sites for the protonation of pyridine. Wolken and Tureček generated gaseous 3-hydroxy-(1H)-pyridinyl radical with femtosecond collisional electron transfer to 3-hydroxy-(1H)-pyridinium cations; several decomposition channels of 3-hydroxy-(1H)-pyridinyl radical that increased with increasing internal energies of 3-hydroxy-(1H)-pyridinium cation were reported.[26] The assignments of the 3-hydroxy-(1H)-pyridinium cation and the 3-hydroxy-(1H)-pyridinyl radical were made according to theoretical calculations, which yielded a proton affinity of 938 kJ mol^{-1} for protonation at the N atom, at least 175 kJ mol^{-1} greater than protonation at other sites.[26, 27] To our knowledge, spectral identification of neither 3-hydroxy-(1H)-pyridinium cation nor 3-hydroxy-(1H)-pyridinyl radical has been reported.

The use of solid *para*-hydrogen (*p*-H_2) as a matrix host generates considerable interest in recent years because of the unique properties of this quantum solid.[28, 29, 30] We have demonstrated that the diminished matrix-cage effect makes feasible a production of free radicals in solid *p*-H_2 via photolysis *in situ* of precursors or via photo-induced bimolecular reactions.[31, 32, 33, 34] We extended this method to use electron bombardment during matrix deposition to produce protonated aromatic compounds and their neutral counterparts.[35,36] We

demonstrated several advantages of this electron-bombardment method in the investigations of protonated benzene ($C_6H_7^+$) and the cyclohexadienyl radical (*c*-C_6H_7),[37] protonated naphthalene (1-$C_{10}H_9^+$ and 2-$C_{10}H_9^+$) and their neutral counterparts,[38] and larger protonated and hydrogenated polycyclic aromatic hydrocarbons (PAH);[39,40,41,42] the method is clean (with negligible fragmentation) and sensitive, and provides spectra covering a wide spectral region with much improved resolution and true IR intensity, as compared with other methods for the spectral investigations of protonated PAH. Golec *et al.* applied this method to produce and to record IR spectra of 1-pyridinuum cation ($C_5H_5NH^+$) and pyridinyl (C_5H_5NH and 4-C_5H_6N) radicals.[43] In this paper, we report the IR absorption spectra of the *trans*-conformers of 3-hydroxy-(1H)-pyridinium cation and 3-hydroxy-(1H)-pyridinyl radical, produced on electron bombardment of a mixture of 3-hydroxypyridine and *p*-H_2 during the deposition of a matrix sample.

II. EXPERIMENTS

The experimental setup has been described previously.[33, 37] The gaseous mixture of 3-C_5H_4(OH)N and *p*-H_2 was deposited onto a gold-plated copper substrate at 3.2 K that also reflects the incident IR beam to the detector. Infrared absorption spectra were recorded with a Fourier-transform infrared (FTIR) spectrometer (Bruker, Vertex 80v) having a KBr beamsplitter and a HgCdTe detector cooled to 77 K to cover the spectral range 450–5000 cm^{-1}. Two hundred scans at resolution 0.25 cm^{-1} were recorded at each stage of the experiment.

We employed electron bombardment during deposition of a gaseous sample of *p*-H_2 containing a small proportion of 3-C_5H_4(OH)N. A mixture of 3-C_5H_4(OH)N/*p*-H_2 (estimated mixing ratio ~10 ppm) was typically deposited at a rate of 13 mmol h^{-1} over a period of 4–8 h.

An electron beam (kinetic energy 200 eV and current 30 μA) from an electron gun (Kimball Physics, Model EFG-7) was employed to bombard the matrix during deposition. To differentiate various products produced under electron bombardment of 3-$C_5H_4(OH)N$/*p*-H_2, we kept the matrix in darkness for ~20 h or performed secondary photolysis using light at 370±10 or 450±10 or 520±15 nm from appropriate light-emitting diodes.

Pure *p*-H_2 was obtained on catalytic conversion of *normal*-H_2 (*n*-H_2); the converter has been described elsewhere.[37] The temperature for conversion of *n*-H_2 to *p*-H_2 was set at ~13 K, giving a proportion of *ortho*-H_2 less than 100 ppm according to the Boltzmann distribution. *Para*-H_2 was passed through the sample container, heated to ~308 K to have sufficient vapor pressure of sample, before the mixture was deposited onto the substrate.

III. QUANTUM-CHEMICAL CALCULATIONS

All calculations employed the Gaussian 09 suite of programs.[44] Geometry optimizations and calculations of vibrational wavenumbers were performed with B3LYP hybrid functionals[45,46] with the aug-cc-pVTZ basis set and the B3PW91 method that uses Becke's three-parameter hybrid exchange functionals and a correlation functional of Perdew and Wang[45,47] with the 6-311++G(2d,2p) basis set. Harmonic vibrational wavenumbers were calculated analytically at each stationary point. The anharmonic vibrational wavenumbers were calculated with a second-order perturbation approach, VPT2.[48] In calculations of relative energies, zero-point vibrational energy (ZPVE) corrections were performed with unscaled harmonic vibrational wavenumbers.

A. 3-hydroxypyridine [3-$C_5H_4(OH)N$]

3-hydroxypyridine has *cis* and *trans* conformers that differ in the orientation of the hydroxyl

(OH) group. *Cis*-3-C_5H_4(OH)N is more stable than *trans*-3-C_5H_4(OH)N by 2.1 kJ mol^{-1} (ZPVE corrected) according to the B3LYP/aug-cc-pVTZ calculations. Important structural parameters of *cis*- and *trans*-3-C_5H_4(OH)N, predicted with the B3LYP/aug-cc-pVTZ method, are presented in Figs. 1(a) and 1(b), respectively; these structures are similar to each other except for the COH angle. Structural parameters of *cis*-3-C_5H_4(OH)N predicted with the B3LYP and B3PW91 methods and those in the literature[11, 19] are compared in Table SI of the supplementary material.

The harmonic, scaled harmonic, and anharmonic vibrational wavenumbers and IR intensities of *cis*- and *trans*-3-C_5H_4(OH)N predicted with the B3LYP and B3PW91 methods are compared with experimental data in Table SII of the supplementary material. The anharmonic vibrational wavenumbers of the six most intense IR lines of *cis*-3-C_5H_4(OH)N, with IR intensities greater than 30 km mol^{-1}, are 3605 (ν_1), 1437 (ν_9), 1250 (ν_{12}), 1203 (ν_{13}), 1161 (ν_{14}), and 219 (ν_{29}) cm^{-1}.

B. Protonated 3-hydroxypyridines

Seven sites for the protonation of each of *trans*- and *cis*-3-hydroxypyridine are possible, one on N atom, one on O atom, and five on C atoms. Important structural parameters of *cis*- and *trans*-3-hydroxy-(1H)-pyridinium cation, *cis*- and *trans*-3-C_5H_4(OH)NH^+, with protonation on the N-atom site are shown in Figs. 1(c) and 1(d). Those of other twelve isomers of protonated 3-hydroxypyridines, predicted with the B3LYP/aug-cc-pVTZ method, are presented in Fig. S1 of the supplementary material. The relative energies of protonated 3-hydroxypyridine isomers predicted with the B3LYP and B3PW91 methods and those in the literature[26] are compared in Table SIII of the supplementary material. In contrast to a more stable *cis*-3-C_5H_4(OH)N, the *trans*-3-C_5H_4(OH)NH^+ is more stable than *cis*-3-C_5H_4(OH)NH^+ by ~3.7 kJ mol^{-1}; other cations

have energy greater than *trans*-3-$C_5H_4(OH)NH^+$ by ~166−266 kJ mol^{-1}. Only the *cis* conformers were considered by Wolken and Tureček.[26]

The scaled harmonic and anharmonic vibrational wavenumbers and IR intensities of *trans*-3-$C_5H_4(OH)NH^+$ predicted with the B3LYP/aug-cc-pVTZ method are listed in Table I; the scaling factor is discussed in Sec. IV-A. The scaled harmonic vibrational wavenumbers of the ten most intense IR lines, with IR intensities greater than 30 km mol^{-1}, are 3612 (ν_1), 3394 (ν_2), 1558(ν_9), 1478 (ν_{10}), 1314 (ν_{13}), 1161 (ν_{16}), 1096 (ν_{17}), 771 (ν_{28}), 665 (ν_{29}), and 388 (ν_{32}) cm^{-1}. A comparison of scaled harmonic and anharmonic vibrational wavenumbers and IR intensities of seven isomers of each *trans*- and *cis*-[3-$C_5H_4(OH)N]H^+$ predicted with the B3LYP method is presented in Table SIV of the supplementary material.

C. Mono-hydrogenated 3-hydroxypyridine

Each 3-hydroxypyridinium cation can be neutralized to a 3-hydroxypyridinyl radical except the 3-pyridylhydroxonium cation (protonated at the O atom), for which the corresponding neutral species is unstable. The structure of *cis*- and *trans*-3-hydroxy-(1H)-pyridinyl radical [formally 3-hydroxy-(1H)-pyridin-1-yl or 3-hydroxy-1λ^5-pyridin-1-yl, 3-$C_5H_4(OH)NH$] with the H atom added onto the N-atom site, predicted with the B3LYP/aug-cc-pVTZ method, is shown in Figs. 1(e) and 1(f); those of other ten isomers of 3-hydroxypyridinyl radicals are shown in Fig. S2 of the supplementary material. The relative energies of 3-hydroxypyridinyl radicals predicted with the B3LYP and B3PW91 methods and those in the literature[26] are compared in Table SV of the supplementary material. *Trans*-3-$C_5H_4(OH)NH$ is more stable than *cis*-3-$C_5H_4(OH)NH$ by 3.6−5.1 kJ mol^{-1}; other radicals have energies greater than that of *trans*-3-$C_5H_4(OH)NH$ by

21−61 kJ mol^{-1}; as is the case of 3-$C_5H_4(OH)NH^+$, only *cis*-conformers of mono-hydrogenated species were considered in the literature.[26]

The scaled harmonic and anharmonic vibrational wavenumbers and IR intensities of *trans*-3-$C_5H_4(OH)NH$ predicted with the B3LYP/aug-cc-pVTZ method are listed in Table II. The anharmonic vibrational wavenumbers of the ten most intense IR lines, with IR intensities greater than 30 km mol^{-1}, are 3652 (ν_1), 1541 (ν_8), 1334 (ν_{11}), 1231 (ν_{13}), 1194 (ν_{14}), 1070 (ν_{16}), 715 (ν_{25}), 690 (ν_{26}), 504 (ν_{29}), and 305 (ν_{30}) cm^{-1}. Scaled harmonic and anharmonic vibrational wavenumbers and IR intensities of another six isomers of each *trans*- and *cis*-3-hydroxypyridinyl radicals predicted with the B3LYP method are compared in Table SVI of the supplementary material.

IV. EXPERIMENTAL RESULTS

A. IR spectra of 3-$C_5H_4(OH)N$/*p*-H_2 matrices

The IR spectrum of a 3-$C_5H_4(OH)N$/*p*-H_2 matrix exhibited intense lines at 3633.4, 1490.0, 1441.6, 1430.1, 1249.7, 1214.0, 803.2, and 704.7 cm^{-1}, and many weaker ones, as shown in Fig. 2(a) and marked with •. The wavenumbers of observed lines, listed in Table SII of the supplementary material, agree with those reported for 3-$C_5H_4(OH)N$ isolated in Ar by Person *et al.*[13] Predicted spectra of *cis*-3-$C_5H_4(OH)N$ and *trans*-3-$C_5H_4(OH)N$ are presented in Figs. 2(b) and 2(c) for comparison. These spectra were simulated according to scaled harmonic vibrational wavenumbers and IR intensities; the derivation of scaling factors is discussed later. The predicted spectra of these two conformers are similar except in region 1100−1600 cm^{-1}. From a comparison of the spectral pattern, we concluded that 3-$C_5H_4(OH)N$ has mostly the *cis*-

conformation; the additional lines (as compared with predicted vibrational fundamentals) observed in this experiment (marked as Δ) are likely due to combination or overtone lines of *cis*-3-C_5H_4(OH)N. We cannot, of course, exclude a possibility that some lines might be due to intense fundamental lines of *trans*-3-C_5H_4(OH)N. Our calculations with the B3LYP/aug-cc-pVTZ method predicted that *cis*-3-C_5H_4(OH)N is more stable than *trans*-3-C_5H_4(OH)N by 2.1 kJ mol^{-1}. Even though the population in a matrix typically reflects the Boltzmann distribution on deposition (near 298 K), on consideration of the *trans*-to-*cis* tunneling isomerization to be discussed later, one expects that the *trans*-conformer isomerizes readily to the *cis*-conformer. Person *et al*. reported IR spectra of complexes of 3-hydroxypyridine with water that show characteristic lines near 3404−3452 cm^{-1};[13] the absence of these lines in our spectra indicates that little water (<< 1 ppm) was present in our sample.

We plotted observed vibrational wavenumbers against predicted harmonic vibrational wavenumbers for *cis*-3-C_5H_4(OH)N in Fig. S3 of the supplementary material. A satisfactorily linear relation was observed; scaling equations $y = 0.9350x + 75.8$ and $y = 0.9764x - 1.2$ were derived for regions above and below 2000 cm^{-1}, respectively; in these equations y is the scaled wavenumber and x is the calculated harmonic vibrational wavenumber. We employed these equations to scale the harmonic vibrational wavenumbers of 3-hydroxypyridine, protonated 3-hydroxypyridine, and mono-hydrogenated 3-hydroxypyridine to compare with anharmonic vibrational wavenumbers and experiment, as listed in Tables I, II, SII, SIV, and SVI of the supplementary material.

Because we could not measure accurately the partial pressure of 3-hydroxypyridine, the mixing ratios of 3-hydroxypyridine in solid *p*-H_2 were estimated according to the method

developed by Tam and Fajardo[49] and by Ruzi *et al*.[50] Harmonic IR intensities calculated with the B3LYP/aug-cc-pVTZ method were used. The path length of the matrix was estimated from the integrated area of the line for transition $S_1(0) + S_0(0)$ of solid *p*-H_2 to be ~1.2 mm. Using the integrated absorbance of lines at 3633.4, 1249.7, and 1197.3 cm^{-1}, we derived a mixing ratio 10±2 ppm for *cis*-3-hydroxypyridine in solid *p*-H_2.

B. IR spectra of electron-bombarded 3-$C_5H_4(OH)N$/*p*-H_2 matrices

After the 3-$C_5H_4(OH)N$/*p*-H_2 mixture was bombarded with electrons during deposition for 6 h, many new features appeared. The difference spectrum obtained on subtraction of the spectrum of a 3-$C_5H_4(OH)N$/*p*-H_2 matrix from the spectrum of the electron-bombarded 3-$C_5H_4(OH)N$/*p*-H_2 mixture is presented in Fig. 3(a); as some intense features of 3-$C_5H_4(OH)N$ cannot be stripped completely, these interfered regions are marked with grey rectangles. To differentiate the absorption features of protonated species from those of the neutral ones, we maintained the matrix in darkness for 20 h to allow diffusion of trapped electrons to react with the cations in solid *p*-H_2. The resultant difference spectrum is shown in Fig. 3(b); lines pointing upward indicate production, whereas those pointing downward indicate destruction. We subsequently irradiated the matrix at 520 nm for ~1 h to differentiate features of various species; photolysis or isomerization of certain species might occur. The observed difference spectrum is shown in Fig. 3(c). Further secondary photolysis was performed with light at 450 nm for 1 h; the difference spectrum is shown in Fig. 3(d).

As shown in Fig. 3, the intensities of nineteen lines, with intense ones at 3594.4, 3380.0, 1610.6, 1562.2, 1319.4, 1193.8, 1167.5, and 780.4 cm^{-1}, decreased after the matrix was

maintained in darkness for 20 h and remained approximately unaltered upon further irradiation at 520 and 450 nm. These features, designated as group A^+, showing a correlated change in intensity at various stages of experiments and in separate experiments, are assigned to the *trans*-3-hydroxypyridinium cation (*trans*-3-$C_5H_4(OH)NH^+$), to be discussed in Sec. V-A. The observed wavenumbers and relative IR intensities of lines in group A^+ are compared with predicted values in Table I.

Nineteen upward-pointing features in Fig. 3(b), with intense ones at 3646.2, 3493.4, 3488.7, 1546.7, 1349.6, 1244.1, 1209.1, 1177.3, 979.8, and 685.2 cm^{-1}, decreased in intensity slightly upon irradiation at 520 nm and much more significantly upon irradiation at 450 nm; they are designated as group A (and highlighted with yellow rectangles for easy recognition) in Fig. 3 and assigned to the *trans*-3-hydroxy-(1H)-pyridinyl radical (*trans*-3-$C_5H_4(OH)NH$), to be discussed in Sec. V-B. The observed wavenumbers and relative IR intensities of lines in group A are compared with predicted values in Table II.

As described in Sec. IV-A, we derived a mixing ratio 10±2 ppm for 3-hydroxypyridine in solid *p*-H_2 after deposition with electron-bombardment. Using the IR intensities predicted for observed lines at 1562.2, 1483.4, and 1319.4 cm^{-1} for *trans*-3-$C_5H_4(OH)NH^+$ and 3646.2, 1546.7, and 1177.3 cm^{-1} for *trans*-3-$C_5H_4(OH)NH$, we estimated the mixing ratios after deposition to be [*trans*-3-$C_5H_4(OH)NH^+$] = (0.35±0.18) ppm and [*trans*-3-$C_5H_4(OH)NH$] = (0.9±0.3) ppm. The variations in mixing ratio as a result of maintaining the sample in darkness for 20 h are Δ[*trans*-3-$C_5H_4(OH)NH^+$] = –(0.22±0.03) ppm and Δ[*trans*-3-$C_5H_4(OH)NH$] = (0.20±0.06) ppm.

V. DISCUSSION

A. Assignment of lines in group A^+ to *trans*-3-$C_5H_4(OH)NH^+$

The observation of the decay of the lines in group A^+ after maintaining the matrix in darkness overnight indicates that the most likely carrier of these lines is one of seven possible isomers of protonated 3-hydroxypyridine because the neutralization of the cations by trapped electrons is expected to occur. In Fig. 4(a) we present the inverted spectrum of Fig. 3(b) so that lines in group A^+ (indicated with red arrows and ○) are pointing upward. In Figs. 4(b)–4(d), we plotted the stick IR spectra of three likely isomers of protonated 3-hydroxypyridine: *trans*-3-hydroxy-(1H)-pyridinium, *cis*-3-hydroxy-(1H)-pyridinium, and 3-pyridylhydroxonium cations, respectively; these spectra were simulated according to the scaled harmonic vibrational wavenumbers and IR intensities predicted with the B3LYP/aug-cc-pVTZ method, listed in Table I and Table SIV of the supplementary material. A comparison of lines in group A^+ with those of other possible protonated *trans*-isomers is presented in Fig. S4 of the supplementary material. Because the predicted spectra of *cis*- and *trans*-conformers are similar, we consider first only *trans*-conformers to identify the protonating site, and then compare the spectra of *cis*- and *trans*-conformers.

All seven predicted spectra show distinct spectral patterns because the additional N–H, C–H, or O−H bonding at various sites has distinct effects on the bonding of the aromatic ring. The observed wavenumbers and relative IR intensities of lines in group A^+ agree satisfactorily with those calculated for the *trans*-3-hydroxy-(1H)-pyridinium cation, Fig. 4(b), but with none of the other six cations, as illustrated in Fig. 4(d) and Fig. S4 of the supplementary material. The

observed line positions and relative intensities of lines in group A^+ are compared in Table I with scaled harmonic and anharmonic vibrational wavenumbers and IR intensities predicted for *trans*-3-$C_5H_4(OH)NH^+$ with the B3LYP/aug-cc-pVTZ method. The five most intense lines observed at 3594.4, 3380.0, 1562.2, 1167.5, and 780.4 cm^{-1} agree with the scaled harmonic (and anharmonic) vibrational wavenumbers predicted at 3812 (3587) for ν_1 (OH stretch), 3394 (3393) for ν_2 (NH stretch), 1558 (1561) for ν_9 (CNH bend), 1161 (1155) for ν_{16} (mixed C4H and C3OH bend), and 777 (784) cm^{-1} for ν_{28} (out-of-plane N1H, C5H, and C6H bend) of *trans*-3-$C_5H_4(OH)NH^+$. The NH-stretching (ν_2) mode observed at 3380.0 cm^{-1} is characteristic of the structure of this cation. The average absolute deviations between the observed and calculated wavenumbers are 9.0 ± 7.9 cm^{-1} for anharmonic vibrational calculations and 9.5 ± 6.7 cm^{-1} for scaled harmonic calculations.

The CH-stretching modes of the protonated species with a proton on the carbon atom are predicted to be in the range 2450−2900 cm^{-1}, as indicated in Figs. S4 of the supplementary material. In this spectral region, we observe no lines with a behavior characteristic of cations. The OH-stretching modes of the cation with protonation on the oxygen atom were predicted to be in the range 3400−3500 cm^{-1}, Fig. 4(d); the two lines observed at 3594.4 and 3380.0 cm^{-1} agree poorly with the prediction. The observed lines in group A^+ are hence assigned to 3-$C_5H_4(OH)NH^+$.

We proceed to compare the spectra of *trans*- and *cis*-3-$C_5H_4(OH)NH^+$. The calculated scaled harmonic and anharmonic vibrational wavenumbers and IR intensities of *trans*- and *cis*-3-$C_5H_4(OH)NH^+$ are compared with observed wavenumbers and relative intensities in Fig. 4 and Table SVII of the supplementary material. The predicted spectra of these two conformers are

similar to each other except for the spectral region 1000–1500 cm^{-1}. For the *trans*-conformer, scaled harmonic wavenumbers (IR intensity in km mol^{-1}) of six most intense lines are predicted at 1478 (40), 1334 (27), 1314 (83), 1182 (15), 1161 (152), and 1096 (34) cm^{-1}, whereas for the *cis*-conformer, the six most intense lines are predicted at 1371 (102), 1343 (27), 1314 (21), 1267 (35), 1159 (148), and 1121 (14) cm^{-1}. In our experiment, the wavenumbers (relative integrated absorbance) of the six most intense lines in this region were observed at 1483.4 (37), 1331.5 (24), 1319.4 (64), 1193.8 (61), 1167.5 (132), and 1107.8 (42) cm^{-1}; the observed spectral pattern agrees much better with that predicted for the *trans*-3-hydroxy-(1H)-pyridinium cation than for the *cis*-3-hydroxy-(1H)-pyridinium cation. Considering that the energy of the *trans*-conformer of 3-$C_5H_4(OH)NH^+$ is 3.6 kJ mol^{-1} smaller than that of the *cis*-conformer and the *cis*-to-*trans* tunneling reaction of the COH-moiety is expected to be facile, an observation of *trans*- rather than *cis*-3-$C_5H_4(OH)NH^+$ is reasonable.

Considering the observed chemical behavior, the agreement of vibrational wavenumbers and relative IR intensities between observed lines in group A^+ and predicted lines for the *trans*-3-$C_5H_4(OH)NH^+$ cation, the absence of some unique features expected for isomers protonated at the other six possible sites, and the predicted relative energies, we assign these new features in group A^+ to the *trans*-3-hydroxypyridinium (3-$C_5H_4(OH)NH^+$) cation, the most stable protonated 3-hydroxypyridine.

B. Assignment of lines in group A to *trans*-3-$C_5H_4(OH)NH$

The intensities of lines in group A increased after the electron-bombarded matrix of 3-$C_5H_4(OH)N$/*p*-H_2 was maintained in darkness for 20 h and decreased upon irradiation at 520

and 450 nm, indicating that the carrier might be a neutral species that dissociates at 520 and 450 nm. We hence expect that the carrier of lines in group A to be an isomer of mono-hydrogenated 3-hydroxypyridine redicals. Similarly to protonated species, we firstly consider the more stable *trans*-conformers and then make a comparison with the *cis*-conformers.

In Fig. 5(a) we present the inverted spectrum of Fig. 3(d), the difference spectrum recorded for the electron-bombarded matrix of 3-C_5H_4(OH)N/*p*-H_2 after secondary photolysis at 450 nm for 1 h; the matrix was maintained in darkness for 20 h and irradiated with light at 520 nm for 1 h before this process. Lines in group A are indicated with red arrows and Δ. In Figs. 5(b)–5(d), we plot stick IR spectra of representative isomers: *trans*-3-hydroxy-(1H)-pyridinyl, *cis*-3-hydroxy-(1H)-pyridinyl, and *trans*-3-hydroxy-(2H)-pyridinyl, respectively; the spectra were simulated according to the scaled harmonic vibrational wavenumbers and IR intensities predicted with the B3LYP/aug-cc-pVTZ method, listed in Table II and Table SVI of the supplementary material. A comparison of lines in group A with those of other possible protonated *trans*-isomers is presented in Fig. S5 of the supplementary material. Similar to protonated 3-hydroxypyridine, the spectral patterns of all six *trans*-conformers are distinct because the additional N–H or C–H bonding at various sites has varied effects on the bonding of the aromatic ring.

As illustrated in Fig. 5 and Fig. S5 of the supplementary material, the observed wavenumbers and relative IR intensities of lines in group A agree satisfactorily with those calculated for the *trans*-3-C_5H_4(OH)NH radical, Fig. 5(b), but with none of the other five *trans*-radicals. The observed positions and relative intensities of lines in group A are compared with scaled harmonic and anharmonic vibrational wavenumbers and IR intensities of 3-C_5H_4(OH)NH predicted with the B3LYP/aug-cc-pVTZ method in Table II. The five most intense lines observed

at 3646.2, 3493.4/3488.7, 1546.7, 1349.6, and 1244.1 cm^{-1} agree satisfactorily with the scaled harmonic (anharmonic) vibrational wavenumbers predicted at 3652 (3613) for ν_1 (OH stretch), 3513 (3350) for ν_2 (NH stretch), 1541 (1527) for ν_8 (C2C3 and C5C6 antisymmetric stretch), 1334 (1331) for ν_{11} (mixed antisymmetric C3C4C5 stretch and C3OH bend), and 1231 (1219) cm^{-1} for ν_{13} (ring deformation and C4H bend). The NH-stretching (ν_2) mode observed at 3493.4 and 3488.7 cm^{-1} is characteristic of 3-C_5H_4(OH)NH; its wavenumber is slightly greater than the value 3380.0 cm^{-1} observed for 3-C_5H_4(OH)NH^+, indicating a slightly stronger N–H bond, consistent with a predicted N–H bond length, 1.002 Å, smaller than that, 1.013 Å, of 3-C_5H_4(OH)NH^+. The average absolute deviations between the observed and calculated wavenumbers are 37 ± 41 cm^{-1} (25 ± 20 cm^{-1} excluding CH-stretching modes of which the deviations are as large as 143 cm^{-1}) for anharmonic vibrational calculations and 12.6 ± 6.8 cm^{-1} for scaled harmonic calculations. The CH_2-stretching modes of other isomers with the additional hydrogen on the carbon atom are predicted in the range 2700−2850 cm^{-1}, as indicated in Fig. S5 of the supplementary material; no line was observed in this spectral region. The observed lines in group A are hence assigned to 3-C_5H_4(OH)NH, with hydrogenation at the N-atom site.

We compare next the spectra of *trans*- and *cis*-3-C_5H_4(OH)NH. The experimental spectrum is compared with predicted IR spectra of *trans*-3-hydroxy-(1H)-pyridinyl and *cis*-3-hydroxy-(1H)-pyridinyl radicals in Figs. 5(b) and 5(c) and Table SVIII of the supplementary material. The predicted spectra of these two conformers are similar except in the spectral region 1000–1400 cm^{-1}. For the *trans*-conformer, the most intense line is predicted at 1334 cm^{-1} (scaled harmonic wavenumber) and three medium lines with one-third of the intensity of the former are predicted at 1231, 1194, and 1167 cm^{-1}. For the *cis*-conformer, five lines with similar intensities are

predicted at 1309, 1228, 1190, 1159, and 1073 cm^{-1}. In our experiment, the most intense line was observed at 1349.6 cm^{-1} and three lines with medium intensities were observed at 1244.1, 1209.1, and 1177.3 cm^{-1}, of which the integrated intensities are approximately one-third that of the most intense line (Table II). The experimental data agree much better with the spectrum predicted for the *trans*-3-hydroxy-(1H)-pyridinyl radical than for the *cis*-3-hydroxy-(1H)-pyridiny radical.

According to our time-dependent density functional calculations (TD-B3LYP/aug-cc-pVTZ), *trans*-3-C_5H_4(OH)NH has low-lying excited states near 643, 518, 427, and 381 nm, as shown in Fig. S6, whereas the first excited state of other isomers lies near 465 nm. Our observations that lines in group A decrease in intensity upon irradiation at 520 and 450 nm are consistent with the predicted excited states of *trans*-3-C_5H_4(OH)NH near 518 and 427 nm.

Considering the observed chemical and photolytic behavior, the agreement of vibrational wavenumbers and relative IR intensities between observed lines in group A and predicted lines for the *trans*-3-hydroxy-(1H)-pyridinyl radical, the absence of some unique features predicted for other isomers with hydrogenation at the C atom, and the calculated thermochemistry showing that *trans*-3-C_5H_4(OH)NH is the most stable isomer, we assigned the observed new features in group A to the *trans*-3-hydroxy-(1H)-pyridinyl radical.

C. Effect of hydroxyl moiety on IR spectra

The stick IR spectra of protonated pyridine $C_5H_5NH^+$ and protonated 3-hydroxypyridine $C_5H_4(OH)NH^+$ in solid *p*-H_2 are compared in Fig. 6, in which the lines due to similar vibrational modes are connected with dotted lines. The IR spectrum of $C_5H_5NH^+$, Fig. 6(a), is characterized

by vibrational modes of four types: the most intense line of the NH stretching mode at 3381.9 cm^{-1}, two lines of the CH stretching modes at 2929.3 and 2965.4 cm^{-1}, several lines of the CC-stretching modes in the region 1450–1650 cm^{-1}, and two lines of the out-of-plane CH/NH bending and ring deformation modes in the region 650–750 cm^{-1}. An introduction of a OH group induced three additional lines associated with the hydroxyl moiety. As shown in Fig. 6(b), intense lines due to vibrational modes involving the motion of the OH group were observed at 3594.4 cm^{-1} (ν_1, OH stretch), 1319.4 cm^{-1} (ν_{13}, mixed CO stretch and ring deformation), and 1167.5 cm^{-1} (ν_{16}, mixed CO stretch and C4H stretch); these lines are marked with *. In spectral region 800–1400 cm^{-1}, several intense lines were induced because molecular symmetry was broken by the OH group; these lines are due to CH- or NH-bending and ring-deformation modes; the predicted IR intensities range from 10 to 150 km mol^{-1}, whereas the predicted IR intensities of these modes in protonated pyridine are less than 10 km mol^{-1}.[43] The wavenumbers of other lines, such as for NH-stretching, CC-stretching, and some CH- or NH-bending and ring-deformation modes remain nearly unaltered.

A similar effect is seen upon OH-substitution for mono-hydrogenated pyridine. The stick IR spectra of hydrogenated pyridine and hydrogenated 3-hydroxypyridine measured in solid *p*-H_2 are compared in Fig. S7 of the supplementary material, in which the lines due to similar vibrational modes are connected with dotted lines. The IR spectrum of mono-hydrogenated pyridine, Fig. S7(a), is characterized by vibrational modes of four types: a line of the NH-stretching mode at 3493.1 cm^{-1}, lines of the in-plane NH- and CH-bending modes at 1447.9 and 1331.6 cm^{-1}, respectively, two lines of the ring- deformation modes at 972.9 and 952.8 cm^{-1}, and lines of the out-of-plane CH-bending and ring-deformation modes in region 600–650 cm^{-1}. As

shown in Fig. S7(b), the IR spectrum of 3-C_5H_4(OH)NH exhibits intense features due to vibrational modes involving motion of the OH group at 3646.2 cm^{-1} (ν_1, OH-stretch), 1425.8 cm^{-1} (ν_{10}, mixed N1H, C2H, C5H, and COH bend), 1349.6 cm^{-1} (ν_{11}, mixed C3C4C5-stretch and COH-bend), and 1090.5 cm^{-1} (ν_{16}, COH bend); these lines are marked with *. In addition to these features, a few lines at 1546.7 cm^{-1} (ν_8, antisymmetric C2C3 and C5C6-stretch), 1177.3 (ν_{15}, mixed in-plane C3H and C6H bend) and 818 cm^{-1} (ν_{20}, ring deformation) became intense through the breaking of symmetry.

D. Mechanism of formation

After deposition of 3-hydroxypiridine/*p*-H_2 mixtures without electron bombardment (Fig. 2), we observed lines of *cis*-3-hydroxypyridine, which is more stable than *trans*-3-hydroxypyridine by 2.1 kJ mol^{-1}. An absence of lines due to the *trans*-conformer is consistent with the population expected from a Boltzmann distribution at 3.2 K, but about 30 % of 3-hydroxypididine is estimated to exist as the *trans*-conformer near 300 K; the *trans*-conformer thus isomerizes to the *cis*-conformer after deposition.

The tunneling isomerization of the hydroxyl group of small carboxylic acids in low-temperature matrices has been extensively investigated.[51,52] In these carboxylic acids, *cis*-conformers have greater energy; the transmission coefficient of *cis*-to-*trans* tunneling isomerization was found to correlate with the effective height of the barrier, which is defined as the barrier height after consideration of vibrational zero-point energies. For example, *cis*-formic acid has an effective barrier height of 32 kJ mol^{-1} and has an experimental decay time ~400 s in an Ar matrix.[53] The effective barrier height for the *trans*-to-*cis* isomerization of 3-

hydroxypyridine is calculated to be 11 kJ mol^{-1} with the B3LYP/aug-cc-pVTZ method, much smaller than that of formic acid. A smaller effective barrier implies that the *trans*-to-*cis* isomerization of 3-hydroxypyridine should be more rapid; only *cis*-3-hydroxypyridine was consequently observed after matrix deposition.

The mechanism for the formation of 3-$C_5H_4(OH)NH^+$ and 3-$C_5H_4(OH)NH$ is similar to that for the formation of $C_5H_5NH^+$ and C_5H_5NH reported previously.[43] The ionization of H_2 on electron impact produces H_2^+; a subsequent rapid and exothermic proton transfer to a nearby H_2 molecule produces H and H_3^+.[54] Although spectral evidence for the formation of H_3^+ has yet to be established, an occurrence of protonated species supports its formation in electron-bombarded *p*-H_2 matrices. Because the proton affinity of 3-$C_5H_4(OH)N$ (929.5 kJ mol^{-1}) is much greater than that of H_2 (422.3 kJ mol^{-1}),[55] H_3^+ thus produced can transfer a proton readily to 3-$C_5H_4(OH)N$ to form 3-$C_5H_4(OH)NH^+$,

$$H_3^+ + 3\text{-}C_5H_4(OH)N \rightarrow 3\text{-}C_5H_4(OH)NH^+ + H_2. \quad (1)$$

The presence of a hydroxyl group does not alter the site of protonation.

The enthalpy of reaction for the formation of 3-$C_5H_4(OH)NH^+$ via protonation on the N-atom site is the most exothermic, protonation on the C-atom sites is less exothermic by 167−265 kJ mol^{-1}, and protonation on the O-atom site is less exothermic by 220 kJ mol^{-1}, as predicted with the B3LYP/aug-cc-pVTZ method (Table SIII of the supplementary material). Our observation of a protonation of 3-hydroxypyridine on the N-atom site, but on neither the carbon nor the oxygen site, is consistent with the prediction that 3-$C_5H_4(OH)NH^+$ is much more stable than other isomers. Protonation of *cis*-3-hydroxypyridine is thought to produce initially *cis*-3-

$C_5H_4(OH)NH^+$, but the large exothermicity of a proton-transfer reaction (~523 kJ mol^{-1} from calculation) facilitates isomerization of *cis*-3-$C_5H_4(OH)NH^+$ to *trans*-3-$C_5H_4(OH)NH^+$ with the dissipation of internal energy to surrounding *p*-H_2 molecules. Moreover, even if *cis*-3-$C_5H_4(OH)NH^+$ were initially stabilized in solid *p*-H_2 upon protonation, a tunneling isomerization reaction would occur readily to convert *cis*-3-$C_5H_4(OH)NH^+$ to *trans*-3-$C_5H_4(OH)NH^+$.

The 3-hydroxy-(1H)-pyridinyl radical, 3-$C_5H_4(OH)NH$, is expected to be formed in the neutralization of 3-$C_5H_4(OH)NH^+$,

$$3\text{-}C_5H_4(OH)NH^+ + e^- \rightarrow 3\text{-}C_5H_4(OH)NH, \quad (2)$$

or in reactions between the H atom and 3-hydroxypyridine,

$$3\text{-}C_5H_4(OH)N + H \rightarrow 3\text{-}C_5H_4(OH)NH \text{ and other isomers.} \quad (3)$$

The observed variation in the mixing ratio after maintaining the matrix in darkness for 20 h is Δ[*trans*-3-$C_5H_4(OH)NH^+$] / Δ[*trans*-3-$C_5H_4(OH)NH$] ≈ -1, indicating that reaction (2) might be a major process during this period. However, because of relatively large errors in estimating the mixing ratios, we do not exclude the occurrence of reaction (3). In separate experiments, reaction of H with pyridine was demonstrated by Golec et al.[43] Moreover, branching ratio during matrix deposition might be different although we are unable to estimate it.

Reaction (2) has no barrier and is highly exothermic; the heat of reaction is ~900 kJ mol^{-1} as inferred from the ionization energy of 3-$C_5H_4(OH)NH$ reported to be 9.2–9.6 eV.[21,56] In contrast, reaction (3) has a barrier for all possible paths. According to our calculations with the B3LYP/aug-cc-pVTZ method, a barrier for the hydrogenation at the N-atom site has height 7.9

kJ mol^{-1}, those at C2, C4, C5, and C6 sites range from 11.7 to 16.1 kJ mol^{-1}, and that at C3 site is 29.5 kJ mol^{-1} (Table SV); a potential-energy diagram associated with the hydrogenation at the N- and C2-atom sites is shown in Fig. S8 of the supplementary material. These results indicate that the hydrogen addition to 3-C_5H_4(OH)N, reaction (3), might occur exclusively at the N-atom site, considering that these reactions proceed through quantum-tunneling at low temperature. Tunneling hydrogenation on an aromatic ring is known to occur for polycyclic aromatic hydrocarbons; e.g., in the case of the hydrogenation of ovalene molecule ($C_{32}H_{14}$), hydrogen addition occurs through a barrier of 9.6 kJ mol^{-1}.[42] Once a tunneling reaction occurs to form *cis*-3-C_5H_4(OH)NH, its exothermicity, ~127 kJ mol^{-1}, is sufficient to overcome a barrier, 10.2 kJ mol^{-1}, for *cis*-to-*trans* isomerization, leading to *trans*-3-C_5H_4(OH)NH. Similarly to 3-C_5H_4(OH)NH$^+$, even if *cis*-3-C_5H_4(OH)NH were temporally stabilized in solid *p*-H_2, it might undergo tunneling isomerization to yield *trans*-3-C_5H_4(OH)NH.

Upon protonation or hydrogenation of 3-hydroxypyridine, the orientation of the OH group for the conformers with the least energy is altered from the *cis* to the *trans* position, according to quantum-chemical calculations. Our experimental observations of only *cis*-3-hydroxypyridine, *trans*-3-C_5H_4(OH)NH$^+$, and 3-C_5H_4(OH)NH at 3.2 K also support that these species are the least-energy conformers. The distinctly preferred orientation of the OH moiety in 3-hydroxypyridine and its protonated or mono-hydrogenated counterparts can be rationalized with electron density distribution. For 3-hydroxypyridine, the N-atom site has more negative charge due to the lone pair, so the OH-moiety that has a more positive terminal hydrogen prefers to be closer to the N-atom site. On the other hand, for 3-C_5H_4(OH)NH$^+$ and 3-C_5H_4(OH)NH, the hydrogen on the N-atom site are more positive, so the hydrogen atom on OH prefer to be away from it. At room

temperature, the OH moiety is nearly freely rotating so it is unlikely to distinguish these two conformers. In a low temperature matrix, we are able to distinguish these conformers through spectral assignments.

VI. CONCLUSION

Electron bombardment on 3-hydroxypyridine/*p*-H_2 mixtures during deposition at 3.2 K produced *trans*-3-hydroxy-(1H)-pyridinium cation, 3-$C_5H_4(OH)NH^+$, and *trans*-3-hydroxy-(1H)-pyridinyl radical, 3-$C_5H_4(OH)NH$; previously unreported IR spectra of these species are characterized. The intensities of lines of 3-$C_5H_4(OH)NH^+$ decreased after maintenance of the matrix in darkness for 20 h, whereas those of 3-$C_5H_4(OH)NH$ increased. Upon secondary photolysis with light at 520 nm, the intensities of lines of 3-$C_5H_4(OH)NH$ decreased, and upon irradiation at 450 nm, became nearly completely diminished.

The spectral assignments were achieved according to the expected chemistry, comparison with quantum-chemically predicted vibrational wavenumbers and IR intensity, and the exothermicity and barrier height of possible reactions predicted with the B3PW91/6-311++G(2d,2p) and/or B3LYP/aug-cc-pVTZ methods. The occurrence of protonation and hydrogenation at the N-atom site of 3-$C_5H_4(OH)N$ is consistent with a theoretical prediction as the most exothermic channel; 3-$C_5H_4(OH)NH^+$ is the most stable isomer and other isomers have energy greater by 172−266 kJ mol^{-1}. That only *trans*-3-$C_5H_4(OH)NH^+$ was observed is consistent with a theoretical prediction that the *trans*-conformer has less energy than the *cis*-conformer by 3.6 kJ mol^{-1}; tunneling reactions to convert the *cis*- to *trans*-conformer are expected to be rapid.

An energy barrier associated with hydrogen addition at the N-atom site, H + *cis*-3-$C_5H_4(OH)N \rightarrow$ *cis*-3-$C_5H_4(OH)NH$, is predicted to be 7.9 kJ mol^{-1}, which is at least 3.8 kJ mol^{-1} smaller than those associated with hydrogenation at the C-atom sites. *Cis*-3-$C_5H_4(OH)NH$ isomerizes to the more stable *trans*-3-$C_5H_4(OH)NH$ because of a rapid *cis*-to-*trans* tunneling isomerization.

SUPPLEMENTARY MATERIAL

See the supplementary material for comparison of optimized structural parameters of *cis*-3-$C_5H_4(OH)N$, predicted and observed vibrational wavenumbers of 3-$C_5H_4(OH)N$, 3-$C_5H_4(OH)NH^+$, and 3-$C_5H_4(OH)NH$, relative energies of protonated 3-hydroxypyridine isomers and mono-hydrogenated ones, predicted wavenumbers of protonated and mono-hydrogenated 3-hydroxypyridine isomers, geometries of isomers of protonated and mono-hydrogenated 3-hydroxypyridine with higher energy, calibration curves used to determine the scaling factors of predicted harmonic vibrational wavenumbers, comparison of the experimental spectrum of lines in group A^+ with predicted spectra of seven possible *trans*-isomers of protonated 3-$C_5H_4(OH)N$, a comparison of the experimental spectrum of lines in group A with predicted spectra of six possible *trans*-isomers of mono-hydrogenated 3-$C_5H_4(OH)N$, a comparison of stick spectra of lines of mono-hydrogenated pyridine, C_5H_5NH, and mono-hydrogenated 3-hydroxy-pyridine, predicted visible absorption spectra of protonated 3-hydroxypyridine isomers, and a potential-energy diagram of the reaction H + 3-$C_5H_4(OH)N$.

ACKNOWLEDGMENTS

This work was supported by Ministry of Science and Technology, Taiwan (grant No.

MOST106-2745-M009-001-ASP and MOST107-3017-F009-003) and the Center for Emergent Functional Matter Science of National Chiao Tung University from The Featured Areas Research Center Program within the framework of the Higher Education Sprout Project by the Ministry of Education (MOE) in Taiwan. Japan Society for the Promotion of Science (JSPS KAKENHI grant No. JP18K03717) partially supported this work. The National Center for High-Performance Computation provided computer time.

TABLE I**.** Comparison of observed vibrational wavenumbers (cm^{-1}) and IR intensities of lines in group A^+ with scaled harmonic and anharmonic vibrational wavenumbers and relative IR intensities of *trans*-3-$C_5H_4(OH)NH^+$ predicted with the B3LYP/aug-cc-pVTZ method.

		Calculations		Experiment	
ν_i	Sym.	Scaled harmonic[a]	Anharmonic	*p*-H_2	Mode description[b]
1	*a′*	3612 (177)[c]	3587 (163)[c]	3594.4 (380)[d]	ν_{OH}
2	*a′*	3394 (163)	3393 (142)	3380.0 (262)	ν_{NH}
3	*a′*	3106 (14)	3106 (10)	3127.2 (13)	ν_{C6H}
4	*a′*	3098 (18)	3095 (30)	3115.7 (13)	ν_{C2H}
5	*a′*	3086 (6)	3066 (7)	3084.3 (9)	ν_{C5H}
6	*a′*	3053 (2)	3041 (2)		ν_{C4H}
7	*a′*	1626 (24)	1625 (8)	1610.6 (57)	*s*-ν_{C2C3}/ν_{C5C6}
8	*a′*	1605 (5)	1601 (7)		*a*-ν_{C2C3}/ν_{C5C6}
9	*a′*	1558 (190)	1561 (169)	1562.2 (190)	δ_{N1H}
10	*a′*	1478 (40)	1484 (33)	1483.4 (37)	*s*-$\nu_{C2N1C6}/\nu_{C3C4C5}$ (*op*)
11	*a′*	1385 (1)	1384 (0)		*a*-$\nu_{C3C4C5}/\delta_{C3OH}/\delta_{NH}$
12	*a′*	1334 (27)	1332 (13)	1331.5 (24)	*a*-$\nu_{C2N1C6}/\nu_{C3C4C5}$
13	*a′*	1314 (83)	1315 (63)	1319.4 (64)	δ_R/ν_{C3O}
14	*a′*	1259 (9)	1269 (11)	1266.1 (7)	$\delta_{N1H}/\delta_{C2H}/\delta_{C6H}$ (*op*)
15	*a′*	1182 (15)	1197 (1)	1193.8 (61)	$\delta_{C2H}/\delta_{C5H}/\delta_{C6H}$ (*op*)
16	*a′*	1161 (152)	1155 (162)	1167.5 (132)	$\delta_{C4H}/\delta_{C3OH}$
17	*a′*	1096 (34)	1105 (57)	1107.8 (42)	δ_R
18	*a′*	1037 (10)	1045 (10)	1042.3 (9)	δ_R
19	*a′*	1012 (3)	1023 (3)		δ_R
20	*a′*	829 (13)	843 (12)	838.0 (15)	δ_R
21	*a′*	620 (0)	629 (0)		δ_R
22	*a′*	535 (2)	546 (2)		δ_R
23	*a′*	398 (14)	401 (14)		δ_{C3O}

24	*a″*	998 (0)	1035 (0)		*oop*-$\delta_{C4H}/\delta_{C5H}$ (*op*)
25	*a″*	947 (2)	951 (3)	925.8 (9)	*oop*-$\delta_{N1H}/\delta_{C2H}/\delta_{C4H}$ /δ_{C6H}
26	*a″*	902 (4)	909 (4)		*oop*-δ_{R}/δ_{C2H}
27	*a″*	832 (1)	838 (2)		*oop*-$\delta_{N1H}/\delta_{C2H}/\delta_{C4H}/\delta_{C5H}$ /δ_{C6H}
28	*a″*	777 (86)	784 (80)	780.4 (67)	*oop*-$\delta_{N1H}/\delta_{C5H}$ /δ_{C6H}
29	*a″*	665 (43)	677 (46)	665.2 (31)	*oop*-δ_{R}
30	*a″*	510 (21)	520 (20)		*oop*-δ_{R}
31	*a″*	401 (7)	413 (73)		*oop*-δ_{R}
32	*a″*	388 (111)	333 (164)		τ_{C3O}
33	*a″*	220 (0)	228 (0)		*oop*-δ_{R}

[a] scaled with equations $y = 0.9350x + 75.8$ and $y = 0.9764x - 1.2$ for values above and below 2000 cm^{-1}, respectively; y is the scaled vibrational wavenumber and x is the calculated harmonic vibrational wavenumber; see text.

[b] approximate mode descriptions, ν: stretching, δ: bending or deformation, δ_R: ring deformation, τ: torsion, *a*: antisymmetric, *s*: symmetric, *ip*: in-phase, *op*: out-of-phase, *oop*: out-of-plane.

[c] IR intensities in km mol^{-1} are listed in parentheses.

[d] Relative IR intensities normalized to that of the most intense line at 1562.1 cm^{-1} are listed in parentheses.

TABLE II**.** Comparison of observed vibrational wavenumbers (cm^{-1}) and IR intensities of lines in group A with scaled harmonic and anharmonic vibrational wavenumbers and relative IR intensities of *trans*-3-C_5H_4(OH)NH predicted with the B3LYP/aug-cc-pVTZ method.

		Calculations		Experiment	
ν_i	Sym.	Scaled harmonic[a]	Anharmonic	*p*-H_2	Mode description[b]
1	*a′*	3652 (61)[c]	3613 (40)[c]	3646.2 (103)[d]	ν_{OH}
2	*a′*	3513 (68)	3350 (6)	3493.4 /3488.7 (82)	ν_{NH}
3	*a′*	3107 (1)	3078 (4)		ν_{C2H}
4	*a′*	3090 (4)	3066 (5)		ν_{C6H}
5	*a′*	3065 (4)	3063 (14)		ν_{C4H}/ν_{C5H} (*ip*)
6	*a′*	3053 (10)	3037 (14)	3067.3 (5)	ν_{C4H}/ν_{C5H} (*op*)
7	*a′*	1623 (10)	1609 (8)		*s*-ν_{C2C3}/ν_{C5C6}
8	*a′*	1541 (43)	1527 (43)	1546.7 (61)	*a*-ν_{C2C3}/ν_{C5C6}
9	*a′*	1450 (6)	1430 (15)	1465.4 (12)	δ_{N1H}
10	*a′*	1419 (23)	1406 (12)	1425.8 (31)	$\delta_{N1H}/\delta_{C2H}/\delta_{C5H}$ (*ip*) /δ_{C3OH}
11	*a′*	1334 (171)	1331 (90)	1349.6 (171)	*a*-$\nu_{C3C4C5}/\delta_{C3OH}$
12	*a′*	1316 (2)	1295 (37)	1295.9 (22)	$\delta_{C2H}/\delta_{C4H}$
13	*a′*	1231 (62)	1219 (64)	1244.1 (68)	δ_R/δ_{C4H}
14	*a′*	1194 (45)	1200 (53)	1209.1 (56)	$\delta_{N1H}/\delta_{C2H}/\delta_{C6H}$ (*op*)
15	*a′*	1167 (44)	1163 (25)	1177.3 (60)	$\delta_{C5H}/\delta_{C6H}$ (*op*)
16	*a′*	1070 (22)	1072 (31)	1090.5 (31)	δ_{C3OH}
17	*a′*	1035 (15)	1025 (4)	1038.3 (27)	*s*-$\nu_{N1C2C3}/\nu_{C4C5C6}$ (*op*)
18	*a′*	1001 (2)	1001 (5)		δ_R
19	*a′*	966 (64)	955 (23)	979.8 (61)	δ_R
20	*a′*	809 (17)	803 (7)	818.0 (21)	δ_R
21	*a′*	588 (0)	582 (4)		δ_R
22	*a′*	519 (1)	505 (2)		δ_R
23	*a′*	389 (9)	364 (8)		δ_{C3O}

24	*a″*	903 (1)	846 (1)		*oop*-$\delta_{C5H}/\delta_{C6H}$ (*op*)
25	*a″*	715 (5)	685 (46)		*oop*-$\delta_{C5H}/\delta_{C6H}$ (*ip*)
26	*a″*	690 (77)	667 (148)	685.2 (57)	*oop*-$\delta_{C2H}/\delta_{C5H}/\delta_{C6H}$ /δ_R
27	*a″*	608 (7)	618 (18)		*oop*-δ_{C2H}/δ_R
28	*a″*	553 (32)	479 (0)	573.8 (35)	*oop*-δ_{C4H}/δ_R
29	*a″*	504 (36)	468 (40)	503.1 (18)	*oop*-δ_R
30	*a″*	305 (64)	236 (70)		*oop*-δ_R/τ_{C3O}
31	*a″*	243 (26)	131 (44)		*oop*-δ_R/τ_{C3O}
32	*a″*	200 (0)	240 (369)		*oop*-δ_R
33	*a″*	77 (63)	1727 (–)		*oop*-δ_{N1H}/δ_R

[a] scaled with equations $y = 0.9350x + 75.8$ and $y = 0.9764x - 1.2$ for values above and below 2000 cm^{-1}, respectively; *y* is the scaled vibrational wavenumber and *x* is the calculated harmonic vibrational wavenumber; see text.

[b] approximate mode description, ν: stretching, δ: bending or deformation, δ_R: ring deformation, τ: torsion, *a*: antisymmetric, *s*: symmetric, *ip*: in-phase, *op*: out-of-phase, *oop*: out-of-plane

[c] IR intensities in km mol^{-1} are listed in parentheses.

[d] Relative IR intensities normalized to that of the most intense line at 1349.6 cm^{-1} are listed in parentheses.

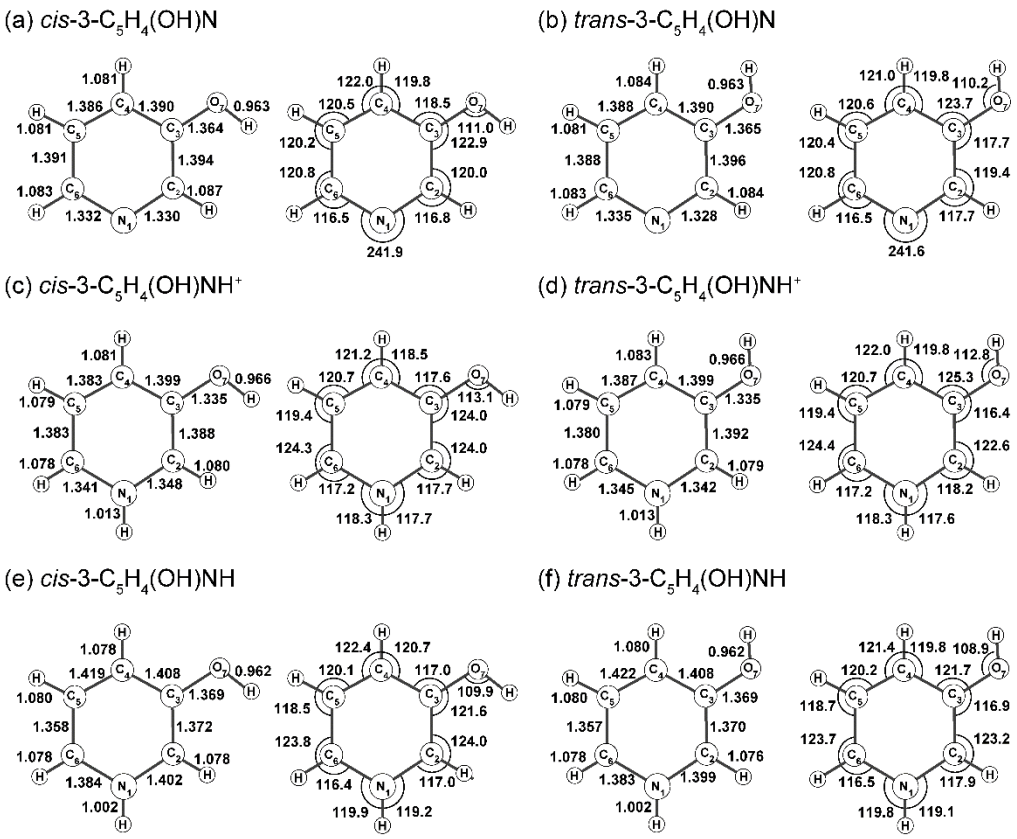

FIG. 1. Geometries of (a) *cis*-3-hydroxypyridine, (b) *trans*-3-hydroxypyridine, (c) *cis*-3-hydroxypyridinium cation, (d) *trans*-3-hydroxypyridinium cation, (e) *cis*-3-hydroxy-(1H)-pyridinyl radical, and (f) *trans*-3-hydroxy-(1H)-pyridinyl radical optimized with the B3LYP/aug-cc-pVTZ method. Bond distances are in Å and bond angles in degree.

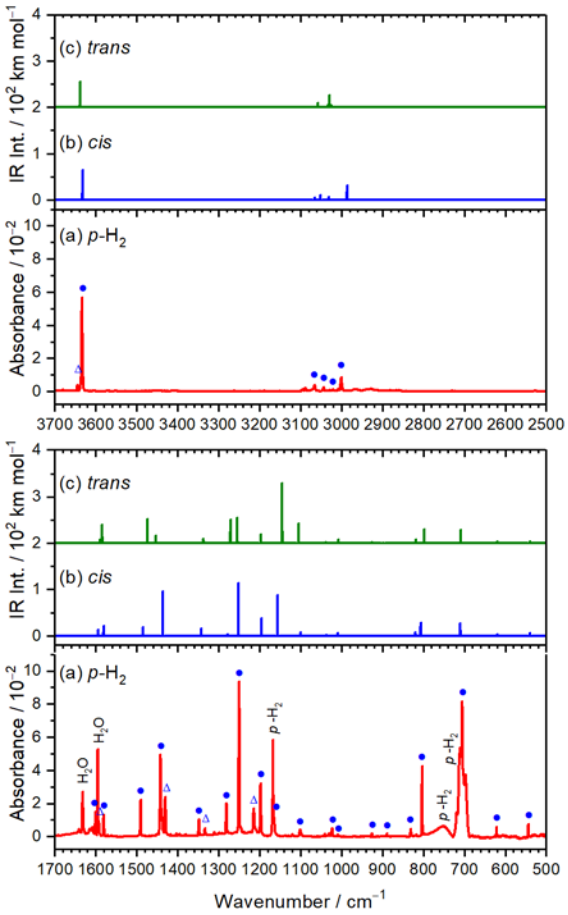

FIG. 2. Comparison of experimental and predicted IR spectra of 3-C_5H_4(OH)N. (a) Spectrum of the 3-C_5H_4(OH)N/*p*-H_2 (~10 ppm) matrix deposited at 3.2 K for 6 h, (b) simulated spectrum of *cis*-3-C_5H_4(OH)N according to scaled-harmonic vibrational wavenumbers and harmonic IR intensities calculated with the B3LYP/aug-cc-pVTZ method, and (c) simulated spectrum of *trans*-3-C_5H_4(OH)N using the same method. In (a), the lines assigned to *cis*-3-C_5H_4(OH)N are indicated with blue dots. Those marked with Δ might be due to overtone or combination transitions of *cis*-3-C_5H_4(OH)N or fundamental transitions of *trans*-3-C_5H_4(OH)N; see text.

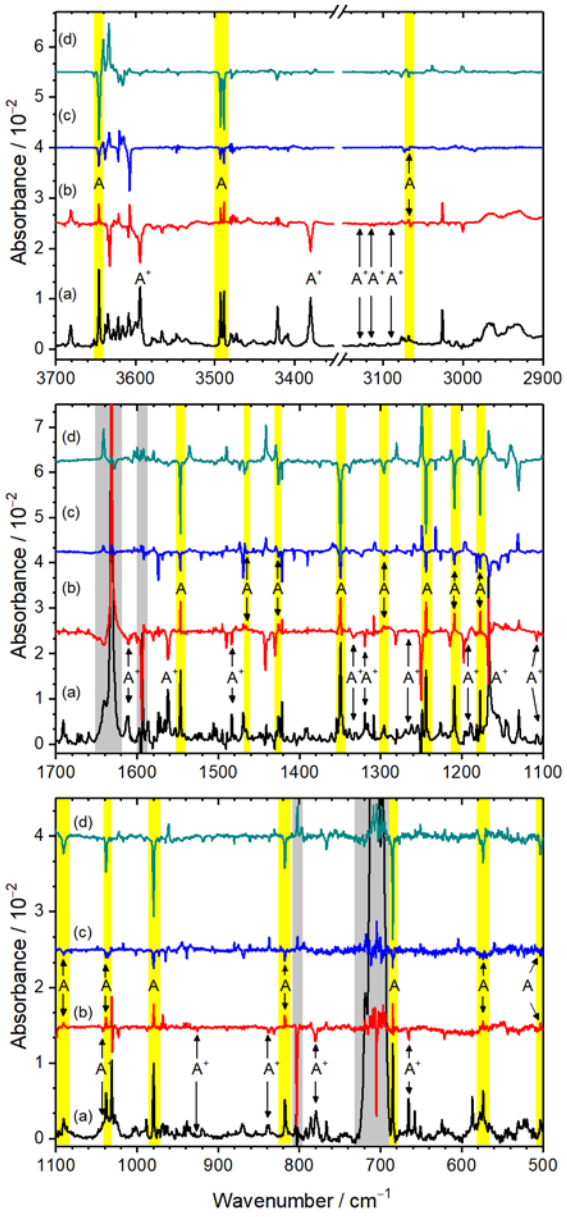

FIG. 3. Difference spectra in regions 3700−2900, 1700−1100, and 1100−500 cm^{-1} after several stages of experiments. (a) 3-$C_5H_4(OH)N$/*p*-H_2 matrix after electron bombardment during deposition at 3.2 K for 6 h with lines of 3-$C_5H_4(OH)N$ stripped; (b) this matrix maintained in darkness at 3.2 K for 20 h; (c) this matrix after irradiation at 520 nm for 1 h, and (d) this matrix after further irradiation at 450 nm for 1 h. In (b)–(d), lines pointing upward indicate production and those pointing downward indicate destruction after the respective experimental procedure. The assignments of lines in each group are A^+: 3-$C_5H_4(OH)NH^+$ and A: 3-$C_5H_4(OH)NH$ (also shaded with yellow). The spectral regions suffering from severe interference from lines of 3-$C_5H_4(OH)N$, H_2O, or *p*-H_2 are shaded in grey.

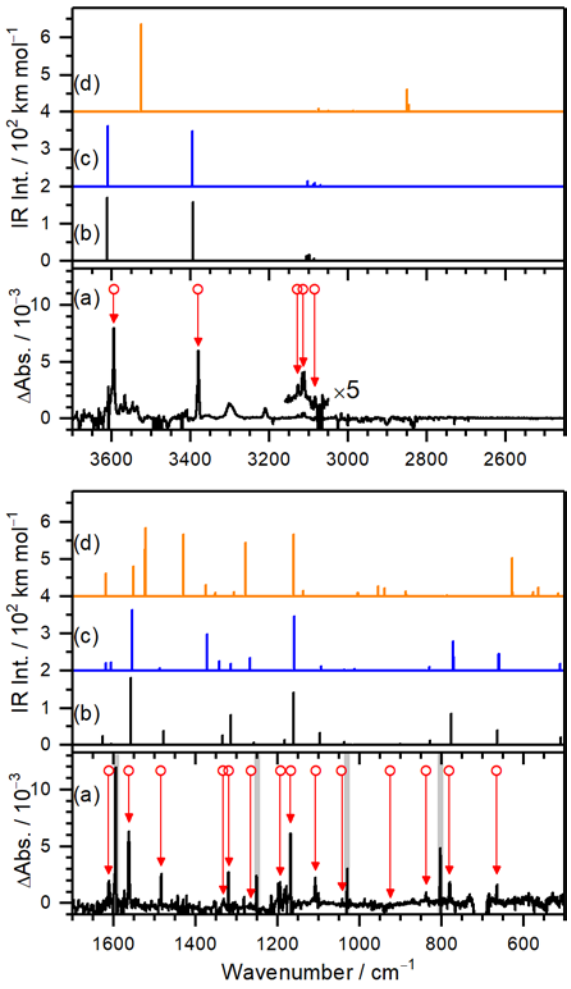

FIG. 4. Comparison of experimental spectrum of lines in group A^+ with simulated spectra. (a) Inverted spectrum of Fig. 3(b), the difference spectrum of the electron-bombarded 3-$C_5H_4(OH)N$/*p*-H_2 sample after being maintained in darkness at 3.2 K for 20 h. Stick IR spectra of (b) *trans*-3-hydroxy-(1H)-pyridinium; (c) *cis*-3-hydroxy-(1H)-pyridinium, and (d) *trans*-3-pyridylhydroxonium 3-$C_5H_4N(OH_2)^+$ cations simulated according to scaled harmonic vibrational wavenumbers and IR intensities predicted with the B3LYP/aug-cc-pVTZ method. In (a), lines in group A^+, indicated with red arrows and ○, are assigned to the *trans*-3-hydroxy-(1H)-pyridinium cation. The spectral regions suffering from severe interference from lines of 3-hydroxypyridine are shaded in grey.

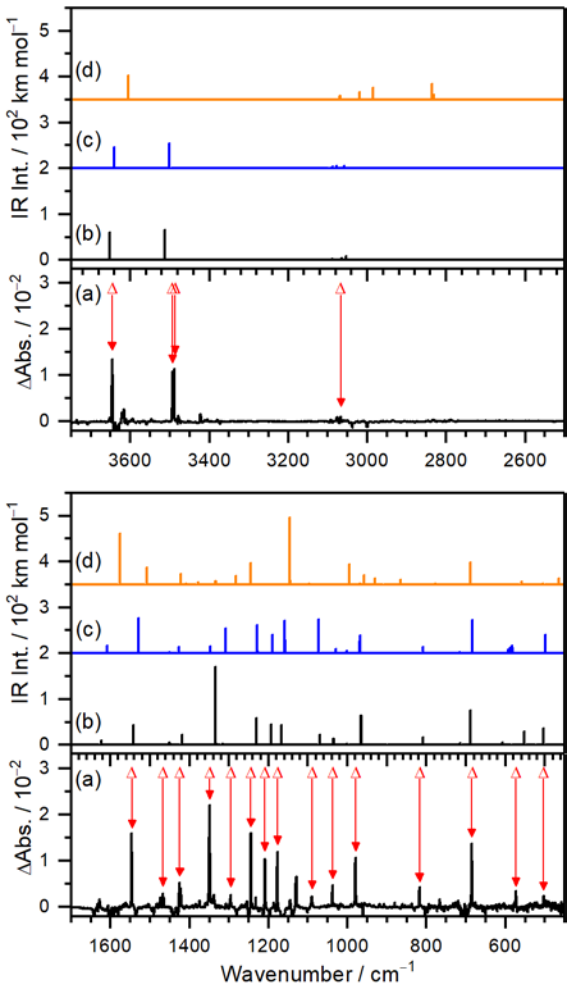

FIG. 5. Comparison of experimental spectrum of lines in group A with simulated spectra. (a) Inverted spectrum of Fig. 3(d), the difference spectrum of the electron-bombarded 3-$C_5H_4(OH)N$/*p*-H_2 sample after secondary photolysis at 450 nm for 1 h. Stick IR spectra of (b) *trans*-3-hydroxy-(1H)-pyridinyl, (c) *cis*-3-hydroxy-(1H)-pyridinyl, and (d) trans-3-hydroxy-(2H)-pyridinyl radicals simulated according to scaled harmonic vibrational wavenumbers and IR intensities predicted with the B3LYP/aug-cc-pVTZ method. Lines in group A, indicated with red arrows and Δ, are assigned to the *trans*-3-hydroxy-(1H)-pyridinyl radical.

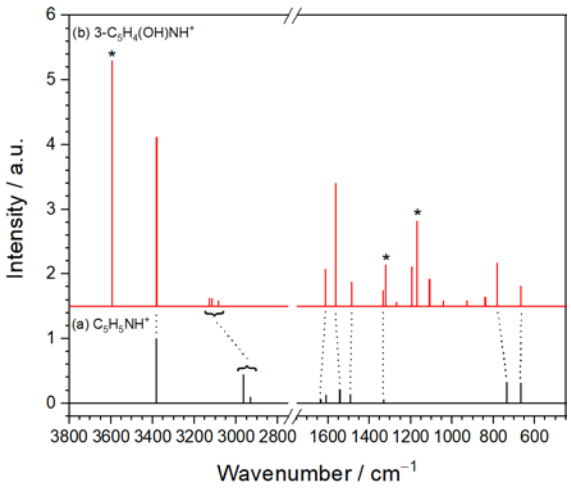

FIG. 6. Comparison of stick spectra of lines of (a) protonated pyridine, $C_5H_5NH^+$, and (b) protonated 3-hydroxy-pyridine, *trans*-3-hydroxy-(1H)-pyridinium cation. The additional lines associated with vibrations of the OH moiety are indicated with *. The dotted lines connect similar vibrational modes.

REFERENCES

[1] G. D. Henry, Tetrahedron, **60**, 6043 (2004).

[2] V. Q. Nguyen and F. Tureček, J. Mass. Spectrom. **32**, 55 (1997).

[3] H. A. Galué, O. Pirali, and J. Oomens, Astron. Astrophys. **517**, A15 (2010).

[4] M. Gallant, M. T. P. Viet, and J. D. Wuest, J. Am. Chem. Soc. **113,** 721 (1991).

[5] P. Beak, Acc. Chem. Res. **10**, 186 (1977).

[6] M. C. Anthony, W. L. Waltz, and P. G. Mezey, Can. J. Chem. **60**, 813 (1982).

[7] N. Tsuchida and S. Yamabe, J. Phys. Chem. A **109**, 1974 (2005).

[8] W. K. Chen, J. Xu, Y. F. Zhang, L. X. Zhou, and J. Q. Li, Acta Phys.-Chim. Sin. **18**, 802 (2002).

[9] R. Sanchez, B. M. Giuliano, S. Melandri, and W. Caminati, Chem. Phys. Lett. **425**, 6 (2006).

[10] D. Vasudevan, P. J. Dorley, and X. Zhuang, Environ. Sci. Technol. **35**, 2006 (2001).

[11] M. J. Scanlan, I. H. Hillier, and A. A. MacDowell, J. Am. Chem. Soc. **105**, 3568 (1983).

[12] J. Wang and R. J. Boyd, Chem. Phys. Lett. **259**, 647 (1996).

[13] W. B. Person, J. E. Del Bene, W. Szajda, K. Szczepaniak, and M. Szczesniak, J. Phys. Chem. **95**, 2770 (1991).

[14] M. J. Scanlan, I. H. Hillier, and R. H. Davies, J. Chem. Soc., Chem. Commun., 685 (1982).

[15] G. La Manna and E. Venuti, J. Comput. Chem. **3**, 593 (1982).

[16] G. La Manna, J. Mol. Struct. THEOCHEM **85**, 389 (1981).

[17] N. Bodor, M. J. S. Dewar, and A. J. Harget, J. Am. Chem. Soc. **92**, 2929 (1970).

[18] R. Sanchez, B. M. Giuliano, S. Melandri, and W. Caminati, Chem. Phys. Lett. **435**, 10 (2007).

[19] F. Buyl, J. Smets, G. Maes, and L. Adamowicz, J. Phys. Chem. **99**, 14967 (1995).

[20] K. C. Mehdi, Indian J. Phys. B **58**, 328 (1984).

[21] M. J. Cook, S. El-Abbady, A. R. Katritzky, C. Guimon, and G. Pfister-Guillouzo, J. Chem. Soc., Perkin Trans. 2, 1652 (1977).

[22] M. A. Baldwin and G. J. Langley, J. Chem. Soc., Perkin Trans. 2, 347 (1988).

[23] A. Maquestiau, Y. van Haverbeke, R. Flammang, H. Mispreuve, A. R. Katritzky, J. Ellison, J. Frank, and Z. Meszaros, J. Chem. Soc., Chem. Commun., 888 (1979).

[24] A. Maquestiau, Y. van Haverbeke, C. De Meyer, A. R. Katritzky, M. J. Cook, and A. D. Page, Can. J. Chem. **53**, 490 (1975).

[25] S. Sharif, O. Sahin, I. U. Khan, O. Büyükgüngör, and W. T. A. Harrison, Crystals **2**, 1253 (2012).

[26] J. K. Wolken and F. Tureček, J. Am. Chem. Soc. **121**, 6010 (1999).

[27] F. Tureček, J. Mass Spectrom. **33**, 779 (1998).

[28] T. Momose, and T. Shida, Bull. Chem. Soc. Jpn. **71**, 1 (1998).

[29] K. Yoshioka, P. L. Raston, and D. T. Anderson, Int. Rev. Phys. Chem. **25**, 469 (2006).

[30] Y.-P. Lee, Y.-J. Wu, R. M. Lees, L.-H. Xu, and J. T. Hougen, Science **311**, 365 (2006).

[31] M. Bahou, C.-W. Huang, Y.-L. Huang, J. Glatthaar, and Y.-P. Lee, J. Chin. Chem. Soc. **57**, 771 (2010).

[32] M. Bahou and Y.-P. Lee, J. Chem. Phys. **133**, 164316 (2010).

[33] J. Amicangelo and Y.-P. Lee, J. Phys. Chem. Lett. **1**, 2956 (2010).

[34] Y.-F. Lee and Y.-P. Lee, J. Chem. Phys. **134**, 124314 (2011).

[35] M. Bahou, P. Das, Y.-F. Lee, Y.-J. Wu, and Y.-P. Lee, Phys. Chem. Chem. Phys. **16**, 2200 (2014).

[36] M. Tsuge, C.-Y. Tseng, and Y.-P. Lee, Phys. Chem. Chem. Phys. **20**, 5344 (2018).

[37] M. Bahou, Y.-J. Wu, and Y.-P. Lee, J. Chem. Phys. **136**, 154304 (2012).

[38] M. Bahou, Y.-J. Wu, and Y.-P. Lee, Phys. Chem. Chem. Phys. **15**, 1907 (2013).

[39] M. Bahou, Y.-J. Wu, and Y.-P. Lee, J. Phys. Chem. Lett. **4**, 1989 (2013).

[40] M. Bahou, Y.-J. Wu, and Y.-P. Lee, Angew. Chem. Int. Ed. **53**, 1021 (2014).

[41] M. Tsuge, M. Bahou, Y.-J. Wu, L. Allamandola, and Y.-P. Lee, Astrophys. J. **825**, 96 (2016).

[42] M. Tsuge, M. Bahou, Y.-J. Wu, L. Allamandola, and Y.-P. Lee, Phys. Chem. Chem. Phys. **18**, 28864 (2016).

[43] B. Golec, P. Das, M. Bahou, and Y.-P. Lee, J. Phys. Chem. A **117**, 13680 (2013).

[44] M. J. Frisch, G. W. Trucks, H. B. Schlegel *et al.*, GAUSSIAN 09, Revision E.01, Gaussian, Inc., Wallingford, CT USA, 2009.

[45] A. D. Becke, J. Chem. Phys. **98**, 5648 (1993).

[46] C. Lee, W. Yang, and R. G. Parr, Phys. Rev. B **37**, 785 (1988).

[47] J. P. Perdew, K. Burke, and Y. Wang, Phys. Rev. B **54**, 16533 (1996).

[48] J. Bloino and V. Barone, J. Chem. Phys. **136**, 124108 (2012).

[49] S. Tam and M. E. Fajardo, Appl. Spectrosc. **55**, 1634 (2001).

[50] M. Ruzi and D. T. Anderson, J. Chem. Phys. **137**, 194313 (2012).

[51] M. Tsuge and L. Khriachtchev, J. Phys. Chem. A **119**, 2628 (2015).

[52] L. Khriachtchev, J. Mol. Struct. **800**, 14 (2008).

[53] M. Petterson, E. M. S. Maçôas, L. Khriachtchev, J. Lundell, R. Fausto, and M. Räsänen, J. Chem. Phys. **117**, 9095 (2002).

[54] M.-C. Chan, M. Okumura, and T. Oka, J. Phys. Chem. A **104**, 3775 (2000).

[55] E. P. L. Hunter and S. G. Lias, J. Phys. Chem. Ref. Data **27**, 413 (1998).

[56] T. Grønneberg and K. Undheim, Org. Mass Spectrom. **6**, 823 (1972).